Triangulating the human torso

A. van Oosterom

Laboratory of Medical Physics, University of Amsterdam, Herengracht 196, Amsterdam, The Netherlands

A simple, continuous, 2-dimensional Fourier representation of closed surfaces is presented. It is applied to the triangulation of the human torso surface for an arbitrary number of triangles. The shape of the torso is described by a radius function expressed in the cylindrical co-ordinates z and ϕ.

A listing of a FORTRAN program is given, performing this triangulation at equi- z and ϕ values. In addition ordered vertex index triples are computed, allowing the determination of the outward normal vector of each triangle.

(Received March 1977)

In some areas of medical research it is of interest to describe the geometry of the human torso numerically. Examples are the computation of dose distributions in radiotherapy (Computers in Radiology, 1972) and the forward- and inverse problem in electrocardiography (Horacek and Ritsema van Eck, 1972). In the latter cases an integral of a weighted, electrical potential over the body surface has to be calculated. The usual approach to this problem is to represent the body surface by a great number of small triangles, the vertices of which lie on the body surface (Horacek and Ritsema van Eck, 1972; Barnard *et al.*, 1967; Ramsey, 1974). The potential is assumed to be constant per triangle and the integral is approximated by performing a summation over the triangles:

$$\int_s w\Phi dS \simeq \sum_{i=1}^{N} w_i \, \Phi_i \, \Delta S_i$$

where w_i = weight
Φ_i = potential
ΔS_i = area
i = triangle index

In some cases the weights depend on the spatial orientation of the surface elements. One then needs both the co-ordinates of the three vertices and the sequence in which these vertices should be entered into the computation of the orientation (outward normal vector) of each triangle (Barnard *et al.*, 1967).

A method will now be given to obtain both data sets for any number of triangles that one may wish to use in approximating the torso surface. A 2-dimensional Fourier representation of the torso shape is employed. As such it is similar to a method described by Guardo (1972); the actual representation used in this paper, however, being different.

The representation uses a radius function expressed in the cylindrical co-ordinates z and ϕ. The Fourier representation for the radius function being obtained, one can compute the co-ordinates of any vertex point as specified by z and ϕ. In the sequel the vertex points are selected in a regular fashion, i.e. at discrete equidistant z levels z_i, $i = 1, M^*$ and equi-partitioned values ϕ_j, $j = 1, N$.

The triangulation is achieved by connecting vertex (z_i, ϕ_j) to vertex (z_i, ϕ_{j+1}), vertex (z_i, ϕ_j) to vertex (z_{i+1}, ϕ_j) and vertex (z_i, ϕ_{j+1}) to vertex (z_{i+1}, ϕ_j); $i = 1, M^* - 1$ and $j = 1, N$. If $j + 1 > N$ $j + 1$ is set to 1. Vertices (z_1, ϕ_j), $= 1, N$ coincide; so do vertices $(z_{M*}, \phi_j), j = 1, N$.

The problem of finding an optimal triangulation as discussed by Keppel (1975) is avoided in this way. Rather than finding an optimal triangulation for a given number of randomly distributed vertex points the method here allows a straightforward increase in the number of triangles used until some desired accuracy is reached.

Recording the torso shape

A special protractor was built for recording the torso shape (**Fig. 1**). It resembles a similar device used by Boineau *et al*, (1967) for recording the torso of a dog. It records the radius $r_i(\phi_j)$ at discrete angles ϕ_j (15° intervals) and at different levels of z_i (1 cm intervals) (see **Fig. 2**). The subject is positioned such that his axis coincides with the z-axis of the recording apparatus. The axis of a subject has been defined as the line running through the centres of two horizontal rectangles enclosing the torso: one at the level of the upper sternal region and one in the lower abdominal region. The half plane through the z-axis and the sternum is chosen as $\phi = 0$. For the radius function $r_i(\phi_j)$ it is assumed that $r_i(\phi_j) \equiv 0$ for $i = 1; j = 1, 24$ at some height $z_1 = 0$ near the base of the neck. Also $r_i(\phi_j) \equiv 0$ for $i = M^*; j = 1, 24$ at a level $z_{M*} = h$ in the lower abdominal region thus truncating the torso. The resulting matrix $r_{i,j} (i = 1, M^*; j = 1, 24)$ has zero elements for $i = 1$ and $i = M^*$ $j = 1, 24$.

Care was taken to record always during a fixed phase of the respiratory cycle.

2-dimensional Fourier representation of the torso

The recorded values $r_{i,j}$ can be considered as the result of a 2-dimensional spatial sampling procedure carried out on the continuous function $r(z, \phi)$. This function is defined over the region $0 \leqslant z \leqslant h$ and $0 \leqslant \phi \leqslant 2\pi$; the samples taken at a regular grid.

The indicated region has a completely natural, periodic extension for values of ϕ outside the interval $(0, 2\pi)$. If one imagines the function to be extended periodically for z values too, one can then represent the function by means of a 2-dimensional Fourier series expansion:

$$r(z, \phi) = \sum_{k=-\infty}^{\infty} \sum_{l=-\infty}^{\infty} \alpha_{k,l} \exp\{i(2\pi kz/h + l\phi)\} \qquad (1)$$

where $\alpha_{k,l}$ are given by:

$$\alpha_{k,l} = \frac{1}{2\pi h} \int_0^{2\pi} \int_0^{h} r(z, \phi) \exp\{-i(2\pi kz/h + l\phi)\} dz \, d\phi \qquad (2)$$

In practice one has to work with a truncated series:

$$r^*(z, \phi) = \sum_{k=-K}^{K} \sum_{l=-L}^{L} \alpha_{k,l} \exp\{i(2\pi kz/h + l\phi)\} \qquad (3)$$

where K and L are set by the desired accuracy and the speed of convergence of the series with the particular function considered. This speed can be increased by introducing the related function $R(z, \phi)$:

$$R(z, \phi) = \sqrt{\left(\frac{h}{2} - z\right)^2 + r^2(z, \phi)}, \qquad (4)$$

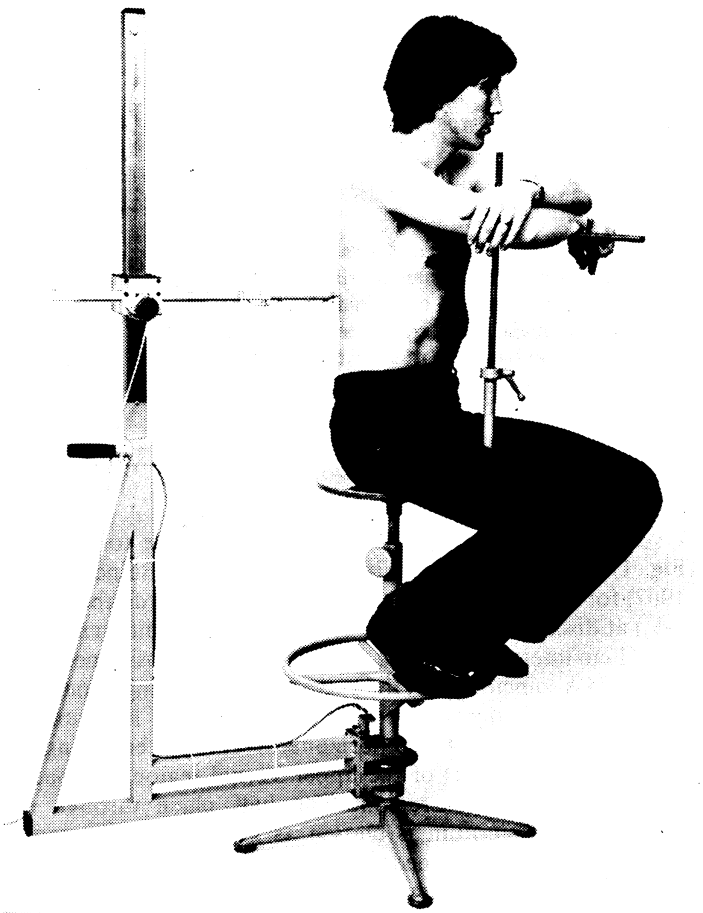

Fig. 1 Protractor recording torso shape

$R(z, \phi)$ being the distance between the surface point (z, ϕ) and the point on the z-axis at $z = h/2$. The expansion coefficients of $R(z, \phi)$ will be denoted $\beta_{k,l}$.

The increased convergence can be demonstrated by considering a spherical surface of radius R_0. One has for this case $r(z, \phi) = r(z) = \sqrt{z(2R_0 - z)}$ which can be expanded as

$$\sqrt{z(2R_0 - z)} = R_0\left\{\frac{\pi}{4} + \sum_{k=1}^{\infty} (-1)^k J_1(k\pi)/k \times \cos(k\pi z/R_0)\right\},$$

in which $J_1(x)$ is the first order Bessel function. In contrast $R(z, \phi) = R(z) = R_0$, which clearly requires a lower order of harmonics. The same effect holds good for sphere-like surfaces and to some extent for the thorax shape.

A further increase in convergence, with an associated decrease in the required value of K, can be achieved by taking the period of the function in the z-direction to be $2h$ rather than h. The function in the region $h < z \leqslant 2h$ will be defined by:

$$R(z, \phi) = h - R(2h - z, \phi)$$

This is an antisymmetric continuation around the value of $R(z, \phi)$ for $z = h$ (Lanczos, 1956). By looking at **Figs. 3**(*a*) and (*b*) the reason for introducing this procedure becomes clear. In Fig. 3(*a*) $R(z, \pi/2)$ is given for an actual torso shape. Here a straightforward periodic continuation is shown. In Fig. 3(*b*) the antisymmetric continuation is depicted.

Since in the antisymmetric case the derivatives of the function at $z = 0, z = h, z = 2h \ldots$ etc. are continuous, the speed of convergence of the series is at least as fast as $1/k^3$ as compared to an original $1/k^2$ (Hamming, 1962).

Finally the function $R(z, \phi)$ can be interpreted as:

$$R(z, \phi) = h/2 + A(z, \phi) \qquad (5)$$

where $A(z, \phi)$ is the deficit to the radius of a sphere just enclosing the torso. (Note that:

$$A(z, \phi) = -A(2h - z, \phi)$$
$$A(0, \phi) = A(h, \phi) = A(2h, \phi) \equiv 0.)$$

The series expansion of $R(z, \phi)$ will be worked out by considering $A(z, \phi)$. The representation will be valid for all shapes (convex, concave, or mixed) for which $R(z, \phi)$ is single valued.

The speed of convergence being increased values for K and L will now be established. A study of $R(z, \phi)$ recorded for widely different torso shapes revealed that values of $K = 25$ and $L = 12$ produced truncation errors in the order of 5 mm. Since the accuracy of the recording procedure, including slight movements of the subjects, was estimated to be of this order, it was concluded that taking $N = 24$ readings at different angles for $M^* = M/2 = 25$ different levels of z provides adequate sampling of the torso shape; $M = 2K$, $N = 2L$.

The multiplicative factors two are governed by the sampling theorem. Just the $M/2$ readings have to be taken because $A(z, \phi)$ has an antisymmetric continuation. Another consequence of the sampling theorem and the periodic extension is that the coefficients of the series expansion of $R(z, \phi)$ can be computed by summation rather than integration:

$$\beta_{k,l} = \frac{1}{MN} \sum_{m=0}^{M-1} \sum_{n=0}^{N-1} R_{m,n}\, E(-km/M - ln/N)$$

with: $R_{m,n} = R(z_m, \phi_n) \qquad m = 0, \ldots, M/2 - 1$

$R_{m,n} = h - R_{M-m,n} \qquad m = M/2, \ldots, M - 1$

$z_m = 2mh/M$

$\phi_n = 2\pi n/N$

$k = 0, \ldots, M - 1$

$l = 0, \ldots, N - 1$

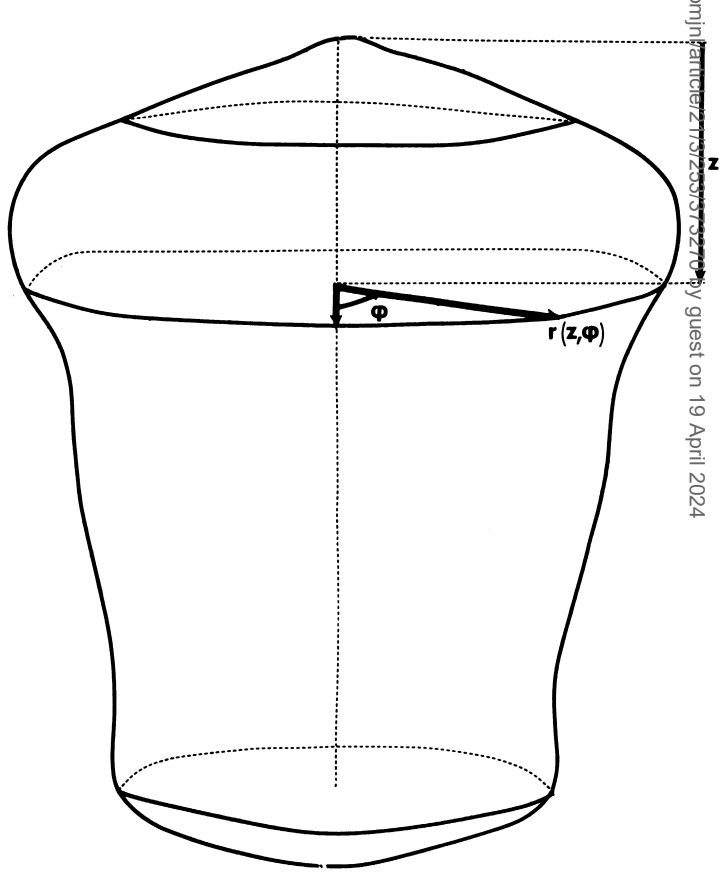

Fig. 2 Specification of $r(z, \phi)$ in the cylindrical co-ordinates used

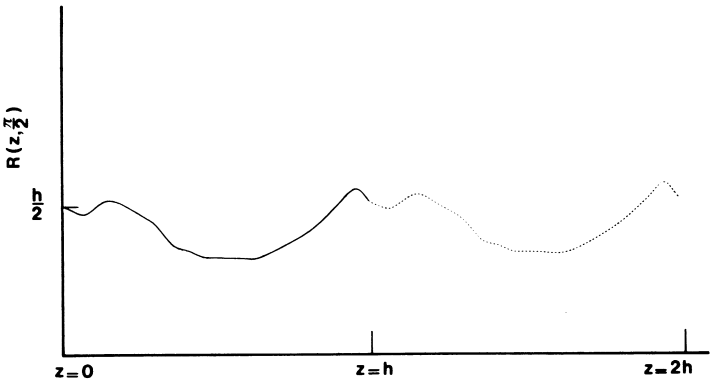

Fig. 3(*a*) Periodic continuation of $R(z,\pi/2)$ period h

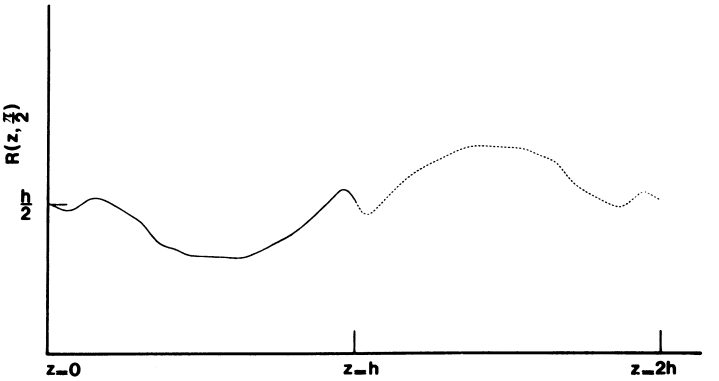

Fig. 3(*b*) Antisymmetric continuation of $R(z,\pi/2)$ period $2h$

$$E(-km/M - ln/N) = \exp\{+2\pi i(-km/M - ln/N)\}$$

The coefficients $\beta_{k,l}$ (spectrum) form the 2-dimensional discrete Fourier representation of the matrix $R_{m,n}$; as such they are periodic:

$$\beta_{k+pM,l+qN} = \beta_{k,l} \qquad p \text{ and } q = 0, \pm 1, \pm 2, \text{ etc.}$$

Moreover, since $R_{m,n}$ is real:

$$\overline{\beta}_{k,l} = \beta_{-k,-l} = \beta_{M-k,N-l}$$

with $\overline{\beta}$ the complex conjugate of $\beta_{k,l}$.

The antisymmetric continuation of the $R_{m,n}$ values around $z = h$ is reflected in the β matrix in the following way:

$$\beta_{0,0} = h/2$$
$$\beta_{0,l} = 0$$

and in general:

$$\beta_{k,l} = \delta_{k,l}\frac{h}{2} - \frac{2i}{MN}\sum_{n=0}^{N-1} E(-ln/N)\sum_{m=0}^{M/2} A_{m,n}\sin(2\pi km/M) \quad (6)$$

with $\delta_{k,l} = 1$ for $k = l = 0$

$\delta_{k,l} = 0$ otherwise

The proof of this is given in Appendix 1.

So far the analysis has resulted in a series expansion of the radius function $R(z, \phi)$:

$$R(z,\phi) = \sum_{k=-K}^{K}\sum_{l=-L}^{L}\beta_{k,l}\exp(\pi ikz/h + il\phi) \quad (7)$$

where $\beta_{k,l}$ can be found using the discrete set of readings $A_{m,n}$ defined in (5) through equation (6). As such (7) can be used for computing the co-ordinates of any point on the surface that one may want to use as a vertex for triangulating this surface.

The expression for $\beta_{k,l}$ can be simplified further if the surface is symmetrical with respect to the plane $\phi = 0$. This symmetry shows up in the $A_{m,n}$ matrix values in the following way:

$$A_{m,n} = A_{m,N-n}$$

Consequently:

$$\sum_{n=0}^{N-1} E(-ln/N)A_{m,n} = A_{m,0} + A_{m,N/2} + 2\sum_{n=1}^{N/2-1} A_{m,n}$$

$$\cos(2\pi ln/N) = \sum_{n=0}^{N/2}(2 - \delta_n - \delta_{n-N/2})A_{m,n}$$

$\cos(2\pi ln/N)$ with $\delta_n = 1$ for $n = 0$

$\delta_n = 0$ otherwise

When this result is substituted in (6) one gets, after changing the order of summation:

$$\beta_{k,l} = \frac{h}{2}\delta_{k,l} - \frac{2i}{MN}\sum_{m=0}^{M/2}\sin(2\pi km/M)\sum_{n=0}^{N/2}(2 - \delta_n - \delta_{n-N/2})\cos(2\pi ln/N)A_{m,n} \quad (8)$$

From this expression it can be learned that:

$\mathrm{Re}\,\beta_{k,l} = 0$ for $k, l \neq 0$

$\beta_{0,l} = 0$ for all $l \neq 0$

$\beta_{k,l}$ is even in l for fixed k

$\beta_{k,l}$ is odd in k for fixed l.

Use of this particular odd and even nature of $\beta_{k,l}$ leads to the following, simplified representation of (7):

$$R(z,\phi) = \sum_{k=0}^{K}\sum_{l=0}^{L}\beta^*_{k,l}\cos(l\phi)\sin(kz\pi/h) \quad (9)$$

In this expression the $\beta^*_{k,l}$'s are now real constants with

$$\beta^*_{0,0} = h/2$$
$$\beta^*_{k,l} = 4i\,\beta_{k,l} \quad l \neq 0, l \neq L$$
$$\beta^*_{k,0} = 2i\,\beta_{k,0} \quad k \neq 0$$
$$\beta^*_{k,L} = 2i\,\beta_{k,L} \quad k \neq 0$$

Relation (9) is the final form of the 2-dimensional Fourier representation of the torso shape that was used in the triangulation.

Triangulation

The continuous form of (9) allows the computation of triangle vertices for any z and ϕ. A FORTRAN program has been written which uses this representation to compute the spatial co-ordinates of triangle vertices at $M^* = M/2$ equidistant values and N-equipartitioned ϕ values.

In all $NVER = N(M^* - 2) + 2$ vertices are computed including top and bottom. In addition, for each of the total of $NTR = 2N(M^* - 3) + N + N = (M^* - 2)2N\,(=2NVER-4)$ triangles, an ordered set of three vertex indices is computed, indicating a clockwise sequence of the three vertex points when the (closed) surface is viewed from the exterior.

A listing of a basic version of this program is given in Appendix 2. A more complete version, including a plotting procedure, will be provided on request.

Results

The above procedure has been used to generate data of triangulated torsos for different degrees of approximation, i.e. for different values of M^* and N. The complete set of coefficients $\beta^*_{k,l}$ (spectrum) that was used in this reconstruction is given in **Table 1.**

An axonometric projection of the resulting shapes is given in **Fig. 4** and **Fig. 5**, respectively for $M^* = 11$, $N = 12$ and for $M^* = 19$, $N = 12$.

At every other z level the vertex points are placed at ϕ values which are shifted over a one half ϕ unit. In this way the resulting triangles have an almost regular equidistant ϕ

Table 1

Full (26 × 13) input matrix $\beta^*_{k,l}$ c.q. $B(k, l)$ of FORTRAN program, specifying torso geometry.

Values given are in cm.

26.000	0.000	0.000	0.000	0.000	0.000	0.000	0.000	0.000	0.000
0.000	0.000	0.000							
-11.054	0.887	-3.218	-0.599	0.268	0.025	-0.025	0.049	-0.166	0.044
-0.101	-0.040	0.049							
0.466	-0.567	-1.413	0.314	0.434	-0.377	0.167	0.085	-0.107	0.103
-0.011	-0.082	0.074							
1.420	0.333	-0.547	0.143	0.240	-0.366	0.065	0.081	-0.061	0.073
0.054	-0.045	0.023							
-0.604	-0.084	-0.142	-0.070	0.195	0.074	-0.127	0.033	0.005	0.007
0.032	0.003	-0.047							
0.177	0.285	0.152	-0.477	-0.025	0.291	-0.248	0.021	0.138	-0.104
0.024	0.086	-0.051							
-0.567	-0.156	0.657	-0.253	-0.004	0.284	-0.177	-0.116	0.160	-0.130
0.027	0.080	-0.040							
0.104	0.256	0.231	-0.327	-0.055	0.204	-0.026	-0.084	0.060	-0.048
-0.006	0.047	-0.021							
-0.244	-0.169	0.186	0.114	-0.115	0.041	0.042	-0.088	-0.018	0.065
-0.036	-0.028	0.009							
0.315	-0.059	-0.105	0.103	-0.075	-0.064	0.135	-0.012	-0.091	0.128
-0.033	-0.067	0.040							
-0.139	-0.183	0.107	0.145	-0.014	-0.111	0.153	-0.003	-0.105	0.094
-0.015	-0.080	0.030							
0.140	-0.047	0.015	0.015	0.001	-0.006	0.061	-0.015	-0.053	0.053
-0.006	-0.047	0.020							
-0.143	-0.102	0.142	0.006	-0.035	0.059	-0.031	-0.032	0.014	0.020
-0.004	-0.025	0.017							
0.125	-0.001	-0.007	-0.037	-0.013	0.052	0.006	-0.006	-0.014	0.001
0.025	0.027	-0.034							
-0.010	-0.052	-0.015	0.024	-0.001	-0.053	0.021	0.023	-0.016	-0.027
0.026	0.040	-0.018							
0.181	0.008	-0.145	0.040	0.043	-0.084	0.026	0.005	-0.025	-0.017
0.035	0.001	-0.004							
-0.021	-0.012	-0.055	0.031	0.039	-0.046	-0.001	0.007	-0.010	-0.012
0.037	0.006	-0.012							
0.118	-0.015	0.000	-0.077	0.030	0.029	-0.042	0.030	-0.007	-0.035
0.030	0.050	-0.027							
-0.101	0.029	0.098	-0.079	0.018	0.049	-0.079	0.012	0.051	-0.045
0.033	0.019	-0.027							
0.017	0.044	0.022	-0.058	0.007	0.037	-0.064	-0.003	0.038	-0.055
0.005	0.028	-0.013							
-0.060	0.017	0.046	0.014	0.019	-0.009	-0.034	0.010	0.009	-0.013
-0.031	-0.010	0.025							
0.061	-0.036	-0.027	0.052	0.012	-0.055	0.020	0.043	-0.004	0.017
-0.053	-0.010	0.035							
-0.013	-0.082	0.015	0.093	-0.006	-0.083	0.053	0.014	0.008	0.042
-0.043	-0.030	0.025							
0.011	-0.063	-0.003	0.080	-0.022	-0.015	0.062	-0.006	-0.015	0.017
-0.050	-0.024	0.031							
-0.058	-0.040	0.072	0.011	-0.008	0.018	0.022	-0.021	0.026	0.021
-0.055	-0.012	0.026							
-0.028	0.005	0.019	-0.015	0.008	0.031	-0.032	0.005	0.026	-0.006
-0.035	0.018	0.020							

arrangement for their centres (see Fig. 4). The figures are constructed by plotting the projections of all composing

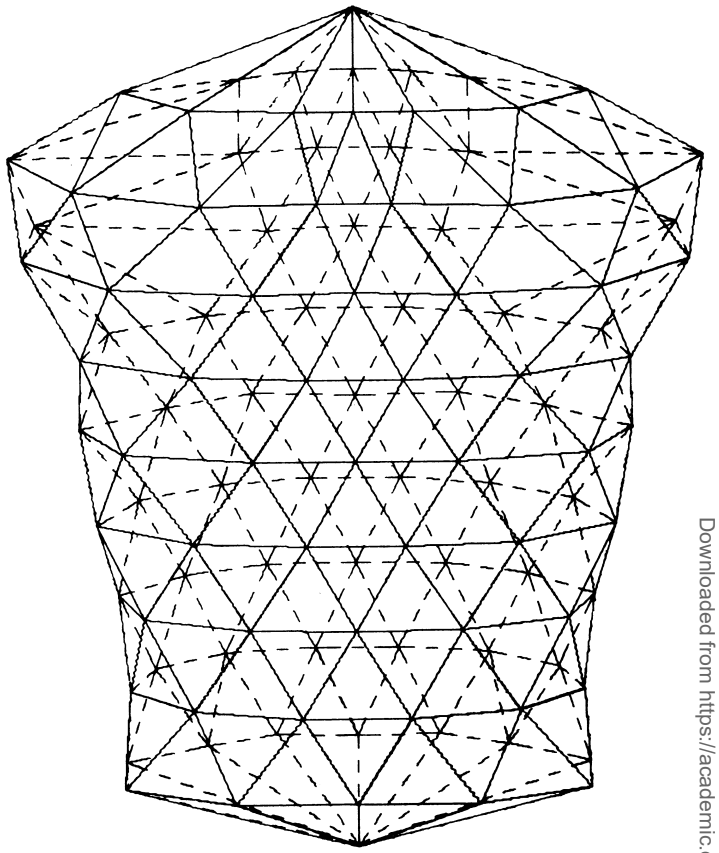

Fig. 5 Triangulation using full spectrum at 19 z-levels and 12 ϕ-positions resulting in 206 vertex points and 408 triangles

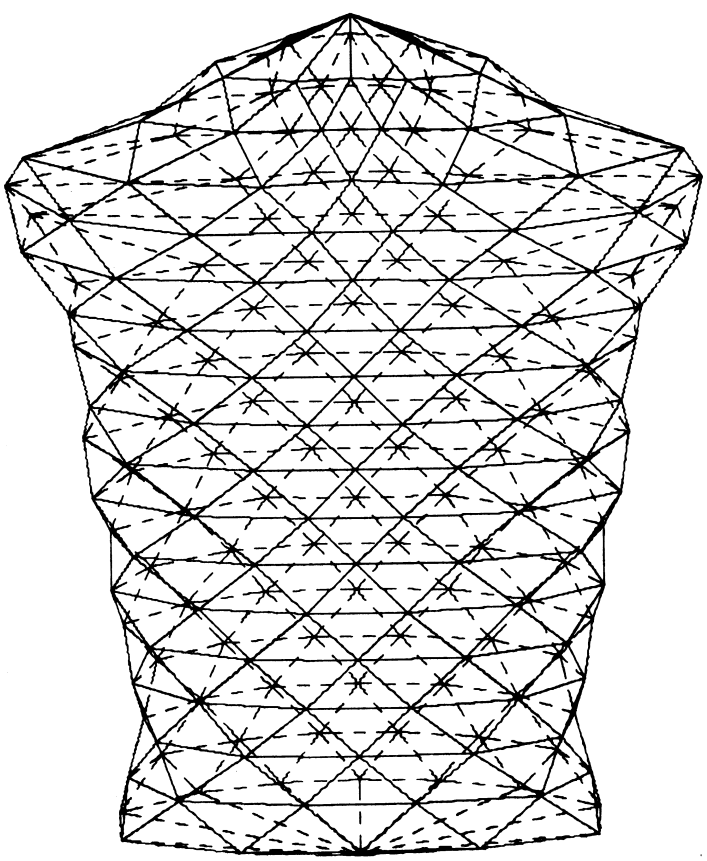

Fig. 4 Triangulation using full spectrum at 11 z-levels and 12 ϕ-positions resulting in 110 vertex points and 216 triangles

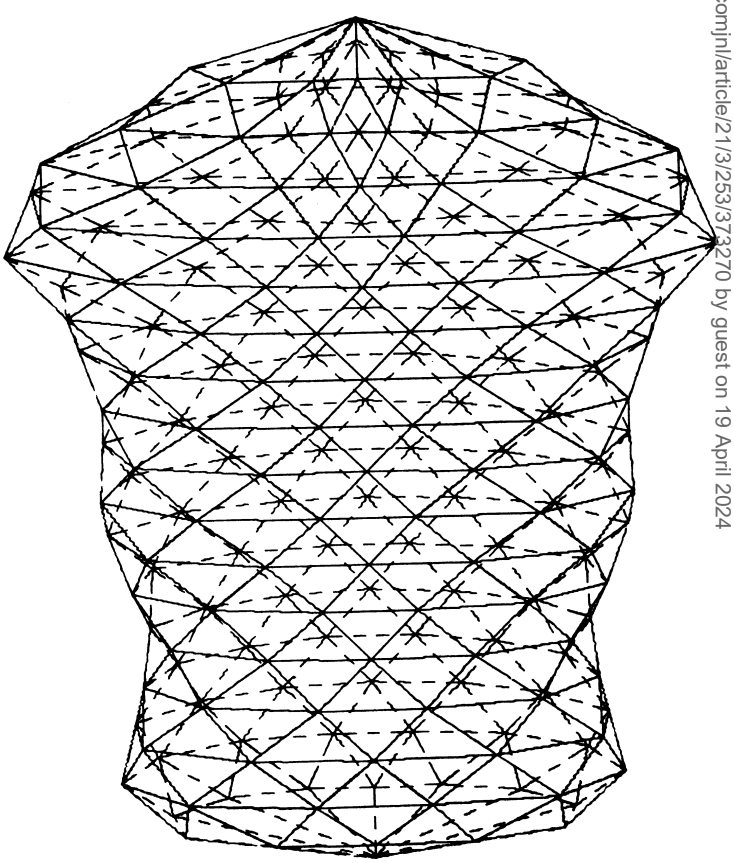

Fig. 6 Triangulation using reduced spectrum

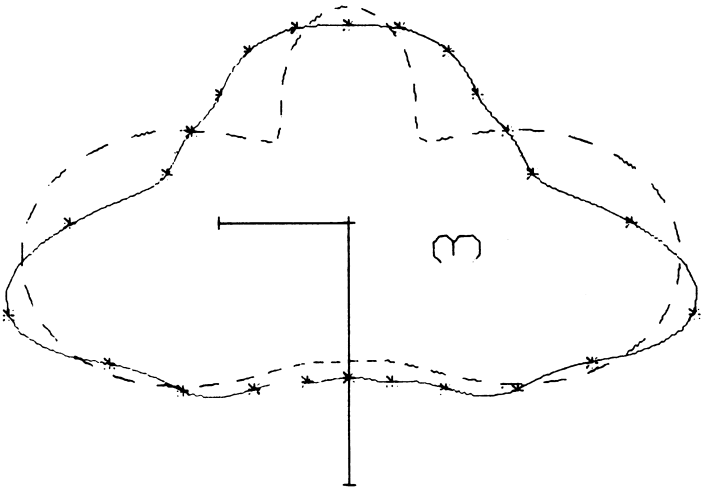

Fig. 7(*a*) *z*-level; base of the neck

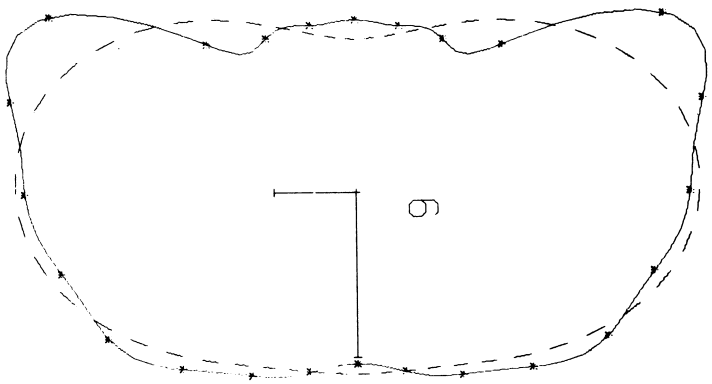

Fig. 7(*b*) *z*-level; just below the armpits

Fig. 7 Reconstruction of $r(z,\phi)$ at various *z*-levels.
Asterisks: recorded values
Continuous line: reconstruction using full spectrum
Dashed line: reconstruction using reduced spectrum
The axes drawn point to the back and to the left

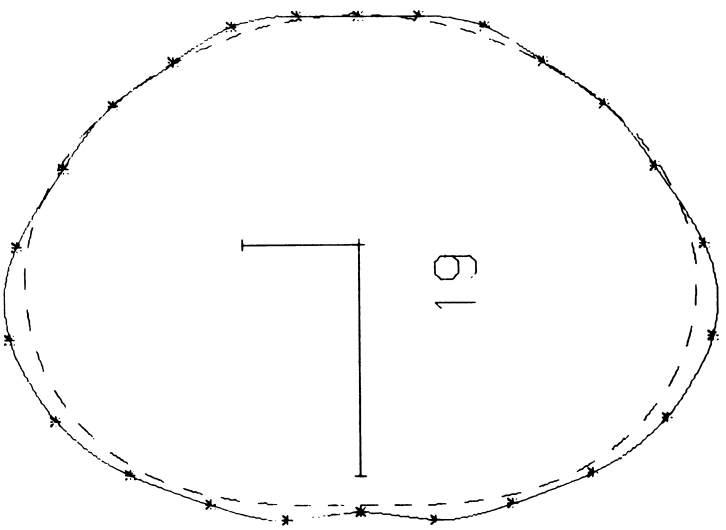

Fig. 7(*c*) *z*-level; just below the sternum

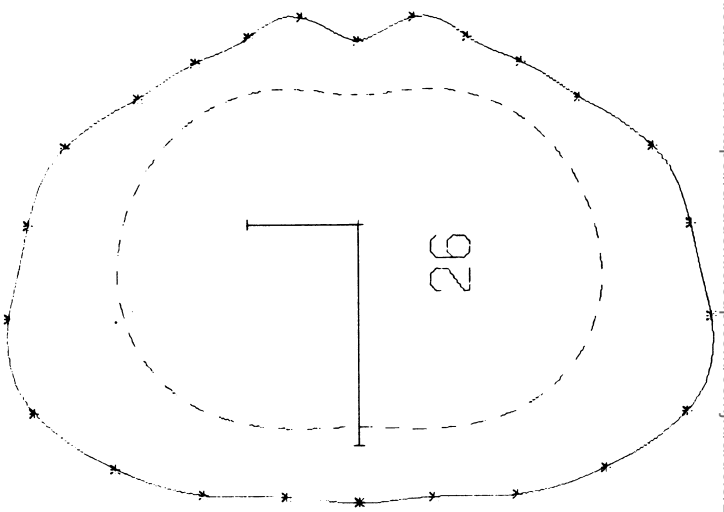

Fig. 7(*d*) *z*-level; 4 cm above lower truncation

triangles. In each plot the 3-dimensional nature of the shapes is enhanced by drawing all frontal triangles by unbroken line segments and all dorsal triangles by dashed line segments. This was achieved in the following way.

When connecting the vertices of a triangle in the (clockwise) sequence as computed previously, two situations will arise. When the triangle is frontal the clockwise sequence is retained in the projection. When the triangle is dorsal the sense of rotation is reversed as a consequence of the projection. In either case the sense of rotation of the plotted triangle can be computed by considering the sign of the outer product of two projected sides, when these projections are considered as (3-dimensional) vectors in the plane of projection. Thus the sign of the vector product will indicate whether a line segment should be unbroken or dashed.

When the size of the input matrix $\beta^*_{k,l}$ is reduced the resulting torso shape is distorted; the more so, the greater the reduction. In **Fig. 6** the values $K = 6, L = 4$ have been used in the reconstruction; while $M^* = 19$ and $N = 12$ as in Fig. 5. The effect of a reduced spectrum is brought out even better in **Fig. 7**(*a*)-(*d*). Here the original measurements of $r(z, \phi)$ are shown by asterisks. The continuous lines are drawn through reconstructed values at 100 equiportioned ϕ values, using (9) and (4) with the full spectrum. The dashed lines are drawn using the reduced spectrum. The *z* levels at which $r(z, \phi)$ is shown are: 7(*a*): base of the neck; 7(*b*): level of the armpits; 7(*c*): just below the sternum; 7(*d*): near the bottom, 4 cm above the truncation.

The reduction of the spectrum predictably affects those parts most where the radius function changes most rapidly (shoulder to neck, truncation at the bottom). The remainder is far less affected and for some applications it may be adequate to use just such simple representation of the thorax shape.

Conclusion

The explicit, continuous representation of closed surfaces by means of the radius function $R(z, \phi)$ allows for the triangulation of these surfaces for any desired number of triangles. The 2-dimensional Fourier representation of $R(z, \phi)$ (7) covers the general case. A more efficient representation is possible when extra symmetry can be assumed (9). In this case the torso can be accurately described using 26 × 13 Fourier coefficients. Limiting the number of coefficients to values as low as 6 × 4 still gives a fair description except for top and bottom.

Acknowledgement

The author wishes to thank Professor Dr J. Strackee and Mr N. Kuyper for their assistance during the study and the preparation of the manuscript.

Appendix 1

To prove relation (6) consider:

$$\beta_{k,l} = \frac{1}{MN} \sum_{m=0}^{M-1} \sum_{n=0}^{N-1} R_{m,n}\, E(-km/M - ln/N)$$

The discrete form of (5) reads:

$$R_{m,n} = h/2 + A_{m,n} \text{ with } A_{m,n} = -A_{M-m,n}\,.$$

Now

$$\beta_{k,l} = \frac{1}{MN} \sum_{m=0}^{M-1} \sum_{n=0}^{N-1} (h/2 + A_{m,n})\, E(-km/M - ln/N)$$

$$= \frac{1}{MN} \sum_{m=0}^{M-1} \sum_{n=0}^{N-1} h/2\, E(-km/M - ln/N) + \frac{1}{MN} \sum_{m=0}^{M-1} \sum_{n=0}^{N-1} A_{m,n}\, E(-km/M - ln/N)$$

$$= \delta_{k,l}\, h/2 + \frac{1}{MN} \sum_{n=0}^{N-1} E(-ln/N) \{ \sum_{m=1}^{M/2-1} A_{m,n}\, E(-km/M) + \sum_{s=M/2+1}^{M-1} A_{s,n}\, E(-ks/M) + A_{0,n}\, E(0) + A_{M/2,n}\, E(-k/2) \}\,,$$

where $\delta_{k,l} = 1$ for $k = l = 0$
$= 0$ otherwise.

In the summation over s the substitution $s = M - m$ is made; subsequent use of $A_{m,n} = -A_{M-m,n}$ and the periodicity of E then results in:

$$\beta_{k,l} = \delta_{k,l}\, h/2 + \frac{1}{MN} \sum_{n=0}^{N-1} E(-ln/N) \sum_{m=1}^{M/2-1} A_{m,n} (E(-km/M) - E(km/M))$$

Since $A_{0,n} = A_{M/2,n} = 0$ for all n. So

$$\beta_{k,l} = \delta_{k,l}\, h/2 + \frac{1}{MN} \sum_{n=0}^{N-1} E(-ln/N) \frac{2}{i} \sum_{m=0}^{M2} A_{m,n} \sin(2\pi k\, m/M)\,. \qquad (6)$$

Appendix 2

```
C FILE DOLLY
C A. VAN OOSTEROM, LAB FOR MED PHYSICS, AMSTERDAM. 15/01/76/
C
C R(Z,FI)=B(1,1)+SUM L=1,LH (SUM K=1,KH (B(K,L)*SIN(Z*(K-1)*PI/LENGTH)))
C *COS((L-1)*FI))
C
      DIMENSION VER(210,3),ITR(410,3),RI(26),B(26,26)
      PI=3.14159265
C INPUT KH AND LH, BOTH LESS THAN 27
      READ(4,10) KH,LH
10    FORMAT(I5)
C INPUT SPECTRUM
      READ(5,20) ((B(I,J),J=1,LH),I=1,KH)
20    FORMAT(F10.5)
      R00=B(1,1)
C INPUT RECONSTR PARAMETERS: KR,LR
      READ(4,10)  KR,LR
      KRM=KR-1
      FPIL=2.*PI/LR
      FPIK=PI/KRM
C TOP VERTEX
      VER(1,1)=VER(1,2)=0.
      VER(1,3)=R00
      ZDIST=2.*R00/KRM
      IND=1
C INTERMEDIATE VERTICES
      DO 60 IZ=2,KRM
      AIZ=IZ-1
      DO 30 L=1,LH
      RI(L)=0.
      DO 30 K=2,KH
      AK=K-1
30    RI(L)=RI(L)+B(K,L)*SIN(FPIK*AIZ*AK)
      AEVEN=IZ-(IZ/2)*2
      HEVEN=AEVEN/2.
      DO 50 JFI=1,LR
      AJFI=JFI
      AJFI=AJFI-1.+HEVEN
      IND=IND+1
      HULP=R00
      FI=FPIL*AJFI
      DO 40 L=1,LH
      AL=L-1
40    HULP=HULP+RI(L)*COS(AL*FI)
      A=R00-AIZ*ZDIST
      RA=SQRT(HULP*HULP-A*A)
      VER(IND,1)=RA*COS(FI)
      VER(IND,2)=RA*SIN(FI)
50    VER(IND,3)=A
60    CONTINUE
      IND=IND+1
C BOTTOM VERTEX
      VER(IND,1)=VER(IND,2)=0
      VER(IND,3)=-R00
      NVER=IND

C DETERM VERTEX INDEX TRIPLES
      DO 70 J=1,LR
      ITR(J,1)=1
      IPT=J+2
      IAPT=IPT
      IF(IPT.GT.LR+1) IAPT=IPT-LR
      ITR(J,2)=IAPT
      ITR(J,3)=IPT-1
70    CONTINUE
      IND=LR
      KMM=KR-2
      DO 90 I=2,KMM
      N0=(I-2)*LR+1
      NEVEN=I-(I/2)*2
      DO 90 J=1,LR
      N1=N0+J
      N2=N1+1
      IF(J.EQ.LR) N2=N2-LR
      N3=N2+LR
      N4=N1+LR
      IF(NEVEN.NE.0) GO TO 80
      IND=IND+1
      ITR(IND,1)=N1
      ITR(IND,2)=N2
      ITR(IND,3)=N4
      IND=IND+1
      ITR(IND,1)=N2
      ITR(IND,2)=N3
      ITR(IND,3)=N4
      GO TO 90
80    IND=IND+1
      ITR(IND,1)=N1
      ITR(IND,2)=N3
      ITR(IND,3)=N4
      IND=IND+1
      ITR(IND,1)=N1
      ITR(IND,2)=N2
      ITR(IND,3)=N3
90    CONTINUE
      N0=(KMM-1)*LR+1
      DO 100 J=1,LR
      N1=N0+J
      IND=IND+1
      ITR(IND,1)=N1
      N2=N1+1
      IF(J.EQ.LR) N2=N2-LR
      ITR(IND,2)=N2
100   ITR(IND,3)=N0+1+LR
      NTRI=IND
      WRITE(6,110) (I,(VER(I,J),J=1,3),I=1,NVER)
110   FORMAT(1X,I4,3F8.4)
      WRITE(6,120) (I,(ITR(I,J),J=1,3),I=1,NTRI)
120   FORMAT(1X,4I4)
      STOP
      END
```


References

BARNARD, A. C. L., DUCK, I. M., LYNN, M. S. and TIMLAKE, W. P. (1967). The application of electromagnetic theory to electrocardiology, *Biophys. J.*, Vol. 7, pp. 463-491.

BOINEAU, J. P., PILKINGTON, T. C., ROGERS, C. L. and SPACH, M. S. (1967). Simulation of body surface potentials. *Digest of the 7th International Conference on Medical and Biological Engineering 1967*, Stockholm, page 412.

Computers in Radiology (1972). Proceedings of the Fourth International Conference on the Use of Computers in Radiation Therapy, Uppsala, Sweden.

GUARDO, R. (1972). The multipole series and locus of the equivalent dipole representing cardiac electrical activity in man, Thesis, Imperial College London.

HAMMING, R. W. (1962). *Numerical methods for scientists and engineers*, McGraw-Hill, page 293.

HORACEK, B. M. and RITSEMA VAN ECK, H. J. (1972). The forward problem of electrocardiography, In: Rijlant, *Proc. Int. Symp. Electrical Field of the Heart*, Presses Académique Européennes, Brussels, pp. 228-238.

KEPPEL, E. (1975). Approximating complex surfaces by triangulation of contour lines. *IBM J. Res. Develop.*, Vol. 2, No. 11, pp. 2-11.

LANCZOS, C. (1956). *Applied analysis*, Prentice Hall, page 216.

RAMSEY, M. (1974). Comparison of epicardial potentials with measured and simulated torso potentials for ventricular depolarisation and repolarisation in the dog, Doctoral Thesis, Duke University.